

High-energy radiation from pulsars: a challenge to polar-cap models

B. Rudak, J. Dyks and T. Bulik

Nicolaus Copernicus Astronomical Center, Warsaw - Toruń, Poland

Abstract. Spectacular results of pulsar observations in X-ray and gamma-ray domains gave a new boost to theoretical models of pulsar magnetospheric activity. A challenging aspect of these efforts is that lightcurves and broadband energy spectra of the brightest HE sources exhibit unexpected richness of features, making each object almost a unique case to be interpreted with a custom-made model. This review offers our subjective account of how the models of high-energy radiation used within the framework of SCLF polar-cap scenarios tackle with these challenges. We describe major characteristics of all radiative processes relevant for modeling the observed features. Then we address successes as well as noticeable disadvantages of these models upon their confrontation with the available data.

1. Introduction

A large fraction of galactic X-ray and gamma-ray sources is associated with neutron stars, in particular with rotation powered pulsars (RPP). Spectacular results of observational campaigns of RPP with ROSAT, ASCA and CGRO, and recently with RXTE and CHANDRA induced a new wave of interest in theoretical models of pulsar magnetospheric activity. A challenging aspect of these efforts is that lightcurves and broadband energy spectra of the brightest HE sources exhibit unexpected richness of features making thus each object a unique case pending special treatment.

The pair creation paradigm is a pivotal element in virtually all models of magnetospheric activity of radiopulsars (which at the moment constitute a vast majority of known RPPs). Electron-positron pairs (e^\pm -pairs) are thought to be responsible for radio emission observed in radiopulsars which is interpreted as the coherent curvature radiation of e^\pm plasma. Pairs can be produced in magnetospheric environments either via photon absorption in a dense field of soft photons (photon-photon collision) or via photon absorption in a strong magnetic field. In either case a supply of hard gamma photons is required in order to fulfill stringent threshold conditions for pair

creation. Not all of these photons would be subject to absorption; many will escape the magnetosphere without any attenuation. This leads us to expect that all radiopulsars (including low- B millisecond objects) should be the sources of gamma radiation. It is up to theoretical models to show whether the expected flux of the radiation is interestingly high with respect to the sensitivity of recent and future gamma-ray telescopes. One should keep in mind, however, that the pair creation paradigm remains just a paradigm for the time being: recently it was questioned by Jessner et al. 2001, who presented arguments that for a wide range of surface temperature, magnetic field strength and spin period, the electrons supplied by neutron star surface via thermionic and field emission will screen out the accelerating electric field \mathcal{E}_\parallel , limiting it to a residual value. In consequence, no favourable conditions would exist for magnetic pair production.

This review offers our subjective account of how the models of high-energy radiation do perform within the framework of polar-cap models with space-charge-limited-flow (SCLF). First, we introduce all ingredients of polar-cap models with SCLF and we describe major characteristics of all radiative processes relevant for physical conditions in pulsar magnetospheres. Then we address successes as well as noticeable disadvantages of these models upon their confrontation with the data.

2. Basic parameters

For the sake of completeness, we recall in this section basic quantities used throughout the review. A neutron star of radius R_s and moment of inertia I , spinning with angular velocity $\Omega = 2\pi/P$ which decreases in time (for whatever the reason) at a rate $\dot{\Omega} = -2\pi P^{-2}\dot{P} < 0$, loses its rotational energy at the rate

$$L_{sd} \simeq 4 \times 10^{31} I_{45} \dot{P}_{-15} P^{-3} \text{erg s}^{-1}, \quad (1)$$

where P is in seconds, $\dot{P}_{-15} \equiv \dot{P}/10^{-15}$ and $I_{45} \equiv I/10^{45} \text{ g cm}^2$, and L_{sd} is the so called spin-down luminosity. If a magnetic dipole is anchored at the center of a neutron star, with its magnetic moment μ_B inclined at angle α to the spin axis Ω , then the strength of the field

at the stellar equator is $B_s = \mu_B/R_s^3$ (and twice as high at the poles). The dipole, rotating in a vacuum will lose energy at the rate

$$L_{\text{magn}} = \frac{2}{3c^3} B_s^2 \sin^2 \alpha R_s^6 \Omega^4. \quad (2)$$

The quantity $B_s \sin \alpha$ can be thus inferred from P and \dot{P} for a neutron star with known values of I and R_s . Another model, where the dipolar radiation is replaced with a magnetospheric wind of particles (Goldreich & Julian 1969), gives a similar result as (2) for an orthogonal case:

$$L_{\text{wind}} \approx \frac{1}{c^3} B_s^2 R_s^6 \Omega^4 \quad (3)$$

and therefore is independent of the angle α . Since no observational support exists for \dot{P} depending on $\sin \alpha$, the standard approach is to apply the latter model ($L_{\text{sd}} = L_{\text{wind}}$) to derive the strength of the dipolar component of magnetic field

$$B_{12}^2 = 10^{15} I_{45} R_6^{-6} P \dot{P} \quad (4)$$

where $B_{12} \equiv B_s/10^{12}\text{G}$, and $R_6 \equiv R_s/10^6\text{cm}$. It is likely that neutron star magnetic fields contain high-order multipoles which may dominate the dipolar component at the surface level. Their relative amplitudes as well as distribution remain, however, unknown. It will be assumed throughout the paper that the magnetic field is a static-like dipole, not distorted by rotational effects or by presence of strong outflowing wind of particles (the latter effect has been recently invoked to decrease very high values of B_s inferred from P and \dot{P} for two SGRs (Harding et al. 1999)). The field is therefore approximated with axisymmetric field lines satisfying $r \sin^2 \theta = R_{\text{dc}}$ in polar coordinates r and θ , with the dipole constant R_{dc} . A dipole constant for which a rigid rotation with the angular velocity Ω reaches the speed-of-light limit (it occurs for $R_{\text{dc}} = c/\Omega$ and this particular value is denoted as R_{lc}) determines the so called light cylinder of radius R_{lc} . All field lines which cross the light cylinder are then considered as open lines, and their foot-points on the stellar surface define two polar caps of radius $R_{\text{pc}} \approx R_s \cdot (R_s/R_{\text{lc}})^{1/2}$, where the latter factor is the sine function of the magnetic colatitude θ_{pc} for the outer rim of the polar cap:

$$\sin \theta_{\text{pc}} = (R_s/R_{\text{lc}})^{1/2}. \quad (5)$$

3. Properties of pulsars in X-rays and gamma-rays

For more than 1500 pulsars known to date only about ~ 40 positive detections in X-rays and no more than 10 detections in gamma-rays have been achieved (Becker 2002, Kanbach 2002). CGRO provided seven high-confidence detections (of *Seven Samurai*) with three other cases classified as ‘likely’ detections. The gamma-ray sources

were identified by virtue of flux pulsations with previously known P and \dot{P} . Crab and Vela are the only pulsars seen by all three instruments of CGRO. No trace of pulsed signal in VHE range (300 GeV – 30 TeV) has been found so far for the gamma-ray pulsars (Sako et al. 2000, Weekes 2000). However, strong steady VHE emission is associated with 3 out of 10 gamma-ray pulsars. Two plerionic sources of the steady VHE radiation – The Crab Nebula and the plerion around B1706-44 – may serve as standard candles, with ‘grade A’ according to Weekes 2000. A third plerion – around the Vela pulsar – was given ‘grade B’ in the same ranking. All 10 gamma-ray pulsars are strong X-ray emitters.

The positions of these HE pulsars are shown in the $P - \dot{P}$ diagram of Fig.1 along with positions of about 700 radio pulsars for which \dot{P} values were available. A remarkable fact is that the location of X-ray sources does not correlate with the inferred strength of magnetic field B_s ; at least not in a naively anticipated way that high-B objects would emit HE radiation, whereas low-B objects would not. In particular, 10 millisecond pulsars – about thirty percent of all millisecond pulsars (the objects with $P \lesssim 0.01\text{s}$ and $\dot{P} \lesssim 10^{-17}$, i.e. with low B values: $B_s \lesssim 10^9\text{G}$) known to date – have been detected as X-ray sources. So far, millisecond pulsars have eluded the detection in gamma rays (possibly with one exception, see below) and just upper limits were available for a handful of them from EGRET observations (Nel et al. 1996). In the case of J0437-4715 the upper limit is interestingly tight – in disagreement with the empirical relation $L_\gamma \propto L_{\text{sd}}^{1/2}$ (see Fig.3).

Empirical evidence that pulsars must somehow tap their high-energy activity from rotation comes from a strong correlation between the success of detection in X and/or γ -rays and the position in the lists of targets ranked by spin-down flux values L_{sd}/D^2 , which is presented in a graphical form in Fig. 2.

Spectral analysis for pulsars detected with ROSAT PSPC (0.1 keV to 2.4 keV) shows that in most cases a power-law spectral model provides acceptable fits to the data (Becker & Truemper 1997). Moreover, an intriguing empirical relation between inferred X-ray luminosity and spin down luminosity was found, $L_X \approx 0.001 L_{\text{sd}}$, confirming rotational origin of most of the X-ray activity. An interesting point is that the relation was obtained for all the sources regardless their temporal characteristics (about 50 % of all pulsars detected with ROSAT are unpulsed sources). A complementary empirical relation was found for pulsed emission from 19 pulsars observed with ASCA (0.6 keV to 10 keV). Assuming opening angle of X-rays to be one steradian, the inferred pulsed X-ray luminosity correlates with spin-down luminosity as

$$L_X = 10^{34} \left(\frac{L_{\text{sd}}}{10^{38} \text{erg s}^{-1}} \right)^{3/2} \text{erg s}^{-1}, \quad (6)$$

according to Saito et al. 1998.

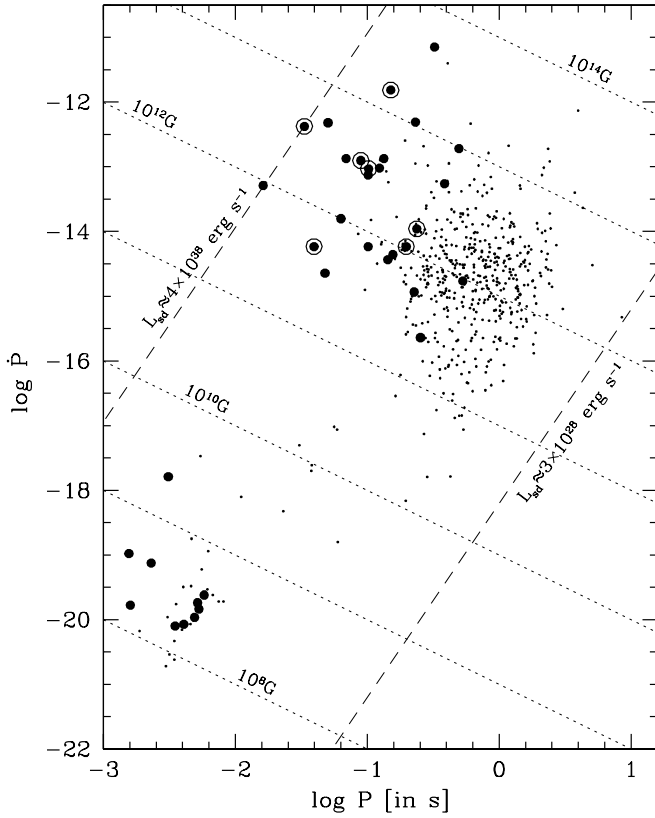


Fig. 1. $P - \dot{P}$ diagram for Rotation Powered Pulsars. The pulsars detected exclusively in radio are indicated with dots; they are taken mostly from the data base of Taylor et al. 1995. Thirty five pulsars emitting X-rays are indicated with bullets. These include two objects recently discovered with RXTE: J0537-6910 in SNR N157B in LMC (Marshall et al. 1998) is the fastest young pulsar known, spinning twice as fast as the Crab pulsar but with similar value of spin down luminosity; J1846-0258 in SNR Kes-75 (Gotthelf et al. 2000), with $P = 0.32$ s, the highest \dot{P} among all RPP. Seven bullets in circles indicate seven gamma-ray pulsars of high confidence. Dashed lines correspond to constant values of spin down luminosity L_{sd} . The upper line ($L_{sd} \approx 4 \times 10^{38} \text{erg s}^{-1}$) includes the Crab pulsar and J0537-6910, the lower one ($L_{sd} \approx 3 \times 10^{28} \text{erg s}^{-1}$) includes J2144-3933 – the slowest ($P = 8.5$ s) radio pulsar detected so far (Young et al. 1999). Dotted lines correspond to constant values of the dipolar component of the surface magnetic field as inferred from P and \dot{P} through (4) with $R_6 = 1$.

A similar power-law empirical relation holds for gamma-rays (cf. Fig.3), but with a different power-law index (e.g. Thompson et al. 1999):

$$L_\gamma \simeq 10^{35} \left(\frac{L_{sd}}{10^{38} \text{erg s}^{-1}} \right)^{1/2} \text{erg s}^{-1}. \quad (7)$$

Important conclusion from (6) and (7) is that neither L_X nor L_γ becomes a sizable fraction of L_{sd} . The most effi-

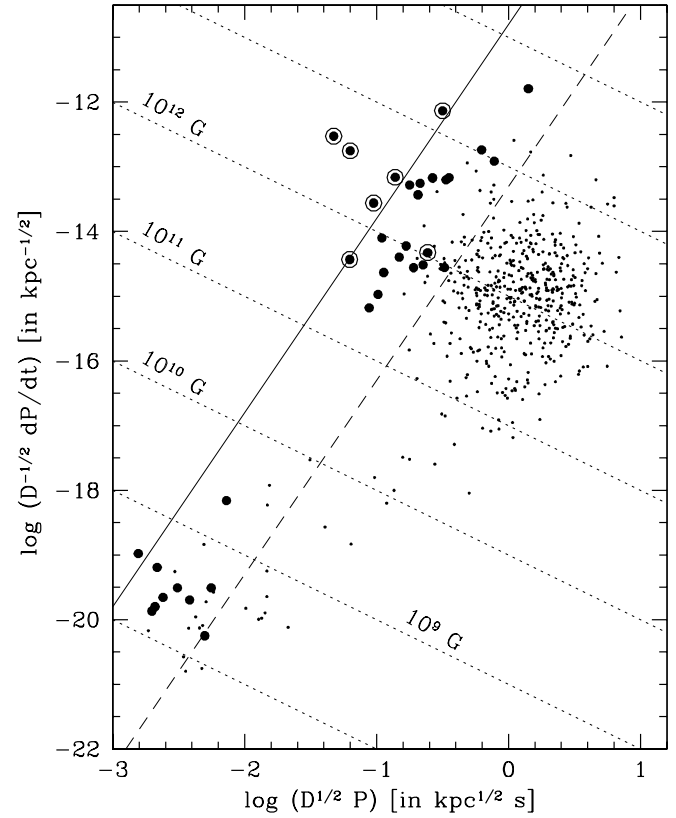


Fig. 2. The ranking of RPPs by their spin-down flux L_{sd}/D^2 . The units of abscissa and ordinate are chosen to keep the resemblance with the $P - \dot{P}$ -diagram: the lines of constant spin-down flux (two such lines - continuous and dashed - are shown as examples) have the same slope with respect to the abscissa (+3) as the lines of constant L_{sd} in Fig. 1; the lines of constant B_s (dotted) have the same slope (-1) with respect to the abscissa in both figures; the range of values for coordinates is also identical. Crab and Vela sticking out well above the continuous line possess the highest spin-down fluxes among the RPPs. The continuous line is trained on B1951+32 with $L_{sd}/D^2 \approx 7 \times 10^{-8} \text{erg s}^{-1} \text{cm}^{-2}$; the dashed line is for the millisecond X-ray pulsar J0751+1807 with $L_{sd}/D^2 \approx 2 \times 10^{-10} \text{erg s}^{-1} \text{cm}^{-2}$. Note a low overall position of the gamma-ray pulsar B1055-52. (From Kluźniak & Rudak 1996, with recent updates).

cient conversion of spin-down luminosity into high-energy radiation is taking place for B1055-52 – the oldest pulsar among *Seven Samurai* – with $L_\gamma \simeq 0.1 L_{sd}$.

High energy lightcurves differ significantly from those in radio. Their most striking feature are relatively long duty cycles as well as phase shifts in comparison to the radio pulses. Only for the Crab pulsar the peaks in gamma-rays as well as in radio wavelengths occur at the same rotational phases. The light-curve shapes fall into two categories. The Crab pulsar, Vela and Geminga show two sharp peaks separated in phase by 0.4 – 0.5 and

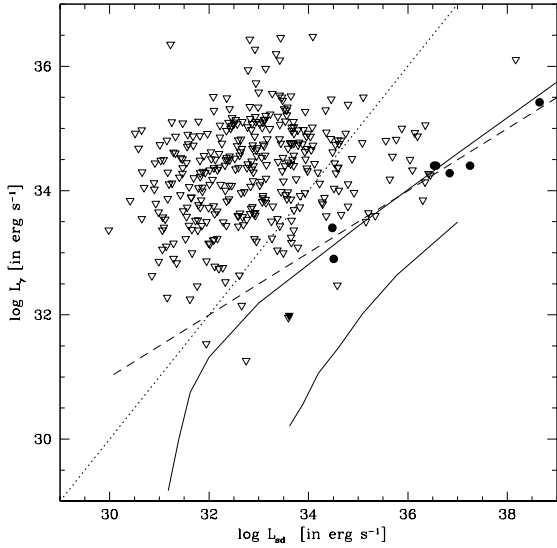


Fig. 3. Gamma-ray luminosity versus spin-down luminosity for seven pulsars (filled dots) detected with the CGRO instruments. Opening angle of one steradian was assumed for the gamma-ray emission. Open triangles are the EGRET upper limits after Nel et al. 1996 for 350 objects, including seven millisecond pulsars. The filled triangle indicates the upper limit for J0437-4715 (Fierro et al. 1995). Note, that most of the upper limits are well above the maximum possible value for L_γ set by $L_\gamma = L_{sd}$ (dotted line). The dashed line marks the empirical relation derived for the CGRO pulsars: $L_\gamma \propto L_{sd}^{1/2}$. Solid lines show evolutionary tracks for a classical pulsar with $B_s = 10^{12}$ G (upper line) and a millisecond pulsar with $B_s = 10^9$ G (lower line) according to the phenomenological model of Rudak & Dyks 1998.

connected by an interpeak bridge of considerable level. B1706-44 shows two peaks separated by 0.2 in phase, with some hints of a third component in between. Other pulsars exhibit broad single pulses. Unknown opening angles for gamma-ray emission introduce a factor of uncertainty when inferring the gamma-ray luminosities. Broad peaks in gamma-ray pulses do not necessarily mean large opening angles for gamma-ray emission. Polar cap models, which rely on purely dipolar magnetic fields postulate nearly aligned rotators, where inclination of magnetic axis to spin axis is comparable to the angular extent of the polar cap (Daugherty & Harding 1994).

With a discovery of sharply peaked pulsed X-ray emission in the fastest millisecond pulsar B1937+21 an apparently separate group of millisecond X-ray pulsars emerges, with its members – B1821-24 (Saito et al. 1997), J0218+4232 (Kuiper et al. 2000), and B1937+21 (Takahashi et al. 2000) – being scaled-down versions of the Crab pulsar as far as sharp pulse profiles and hard power-law X-ray spectra are concerned. An astonishing common feature within the group is the same strength

of the magnetic field estimated at the light cylinder and the fact that it matches the strength of the Crab pulsar magnetic field at the light cylinder.

It is, however, lightcurves and broadband energy spectra extending from optical to X-rays and to gamma-rays, available for *Seven Samurai* (e.g. Thompson et al. 1999, Thompson 2001) that are particularly impressive and challenging for any models of pulsar activity. These observations are reviewed in details by Kanbach 2002 (this volume).

4. Unipolar induction

Consider a neutron star of radius R_s and surface magnetic field B_s as a perfect conductor. For the rotating star with its dipolar magnetic field immersed in a vacuum an external quadrupole electric field \mathcal{E} develops, with non-zero component along magnetic field lines at the surface. The corresponding electrostatic potential Φ in polar coordinates r and θ reads (Michel 1991)

$$\Phi(r, \theta) = -\frac{Q}{r^3} (3 \cos^2 \theta - 1), \quad (8)$$

where $Q = \pi B_s R_s^5 / (3cP)$ is the quadrupole moment. Maximal electromotive force will then be induced between the pole of the star and the outer rim of the polar cap due to:

$$\Delta\Phi_{pc} = \Delta\Phi_{equator} \left(\frac{R_{pc}}{R_s} \right)^2, \quad (9)$$

where

$$\Delta\Phi_{equator} = \frac{1}{2c} B \Omega R_s^2 \quad (10)$$

denotes a (huge but unavailable) potential drop between the pole and the equator. In terms of voltage, polar caps offer then $\Delta V_{pc} \approx 7 \times 10^{12} B_{12} P^{-2}$ Volt

4.1. Potential drops in SCLF gaps

Potential drop (9) sets a firm upper limit for all (model-dependent) realistic potential drops $\Delta\Phi_{||}$, including vacuum gap model of Ruderman & Sutherland, as well as outer gap models of e.g. Cheng et al. 1986. In fact,

$$\Delta\Phi_{||} \ll \Delta\Phi_{pc} \quad (11)$$

for most cases. We will concentrate hereafter on a class of models where the supply of charged particles from a neutron star surface along open field lines is not limited by either binding or cohesive energy of the particles and therefore can reach the Goldreich-Julian rate close to the surface (‘Space Charge Limited Flow’ – Sturrock 1971, Arons & Scharlemann 1979). A concise but to-the-point account of essential properties of the SCLF models has been presented by Arons 2000.

Three boundary conditions essential to the electro-dynamics above the polar cap are (Muslimov & Tsygan 1992):

- 1) $\mathcal{E} \cdot \mathbf{B} = 0$ for the magnetosphere within the closed field lines,
- 2) $\Phi = 0$ at the surface and at the interface between the closed magnetosphere and the open field lines,
- 3) $\mathcal{E}_{\parallel} = 0$ at the surface level,

where \mathcal{E}_{\parallel} is the electric field component parallel to the magnetic field.

Last but not least, it is assumed that the outflow is stationary and the magnetosphere remains axisymmetric.

The electric field \mathcal{E} required to bring a charged particle into corotation satisfies the following equation

$$\mathcal{E} + \frac{1}{c}((\boldsymbol{\Omega} - \boldsymbol{\omega}_{\text{LT}}) \times \mathbf{r}) \times \mathbf{B} = 0 \quad (12)$$

where the inertial-frame dragging effect is included (Beskin 1990, Muslimov & Tsygan 1992) with $\boldsymbol{\omega}_{\text{LT}} = \kappa_{\text{g}}(R_{\text{s}}/r)^3 \boldsymbol{\Omega}$, where $\kappa_{\text{g}} = I/(M_{\text{s}}R_{\text{s}}^2) \cdot R_{\text{g}}/R_{\text{s}}$, and $R_{\text{g}} = 2GM_{\text{s}}/c^2$.

Charge density necessary to support this local \mathcal{E} is

$$\varrho_{\text{corot}} = \frac{1}{4\pi} \boldsymbol{\nabla} \cdot \mathcal{E} \approx -\frac{\boldsymbol{\Omega} \cdot \mathbf{B}}{2\pi c} [1 - \omega_{\text{LT}}] \quad (13)$$

The charge density ϱ_{corot} due to SCLF at $r = R_{\text{s}}$ is called the Goldreich–Julian charge density:

$$\varrho_{\text{GJ}} \approx -\frac{\boldsymbol{\Omega} \cdot \mathbf{B}}{2\pi c} [1 - \kappa_{\text{g}}]. \quad (14)$$

As charged particles flow out along the open field lines a deviation of the local charge density ϱ_{local} from the local corotation density ϱ_{corot} develops. By using now two relations satisfied in the dipolar structure, $B(r) \propto r^{-3}$ and $\varrho(r) \propto r^{-3}$, one obtains a simple formula for local deviation from the corotation charge density:

$$\varrho_{\text{local}} - \varrho_{\text{corot}} \approx \frac{\boldsymbol{\Omega} \cdot \mathbf{B}}{2\pi c} \kappa_{\text{g}} \left[1 - \left(\frac{R_{\text{s}}}{r} \right)^3 \right]. \quad (15)$$

Accordingly, the accelerating potential drop in SCLF reads

$$\Delta\Phi_{\parallel} \approx \Delta\Phi_{\text{pc}} \kappa_{\text{g}} \left[1 - \left(\frac{R_{\text{s}}}{r} \right)^3 \right], \quad (16)$$

where $\Delta\Phi_{\text{pc}}$ is given by (9) and $\kappa_{\text{g}} = 0.15 I_{45}$. This is a remarkable result obtained by Muslimov & Tsygan 1992: the potential drop due to inertial-frame dragging is significantly larger than the drop induced by curvature of magnetic field lines (‘flaring’, Arons & Scharlemann 1979), or – useless to say – by particle inertia (Michel 1974)).

5. Electric field structure in SCLF gaps

The model with frame dragging effects presented in a simplified form above, does not take into account possible

feed-back effect due to e^{\pm} -pairs formed via photon absorption within open magnetic field lines. Copious pair creation occurs in a relatively thin layer – a pair formation front (PFF). The creation of pairs leads to the screening of the accelerating field \mathcal{E}_{\parallel} within the layer of PFF. A detailed picture of this effect would require to follow the dynamics of electrons and positrons in a self-consistent way. Instead, it is reasonable to assume, that the field is shorted out at the height where the first e^{\pm} -pair is created (hereafter denoted as h_c): $\mathcal{E}_{\parallel} = 0$ for $h \geq h_c$.

The problem of electric field structure in the context of SCLF with boundary condition $\mathcal{E}_{\parallel} = 0$ set at $h_0 = 0$ (stellar surface) and at $h \geq h_c$ (PFF) was formulated and solved by Harding & Muslimov 1998a. The solution is rather lengthy and includes special functions. It is however possible to obtain simple but quite accurate analytical approximations. As long as the length h_c of the accelerator is of the order of polar cap radius R_{pc} , the accelerating electric field may be approximated according to Dyks & Rudak 2000a as

$$\mathcal{E}_{\parallel} \approx -1.46 \frac{B_{12}}{P^{3/2}} h \left(1 - \frac{h}{h_c} \right) f_1(\xi) \cos \chi \text{ Gauss}, \quad (17)$$

where $B_{12} = B_{\text{s}}/10^{12}\text{G}$, P is the spin period in seconds, χ is the angle between the spin axis and the magnetic moment of the rotating star, h is expressed in cm, and $M = 1.4 M_{\odot}$, $R_{\text{s}} = 10^6\text{cm}$. The magnetic colatitude $\xi \equiv \theta/\theta(\eta)$ is scaled with the half-opening angle of the polar magnetic flux tube $\theta(\eta)$, where $\eta \equiv 1 + h/R_{\text{s}}$. The magnetic colatitude function $f_1(\xi)$ is a monotonically decreasing function, with $f_1(0) \simeq 1$ and $f_1(1) = 0$.

Vertical structure of the electric field depends (via the location of PFF) on radiative processes which induce the pair creation: curvature radiation (CR) and inverse Compton scattering (ICS) on soft X-ray photons from the stellar surface (brief characteristics of these processes is presented in the next section).

An interesting way to avoid immediate screening of the electric field by created pairs, relevant in strong magnetic fields $\gtrsim 0.1 B_{\text{crit}}$, was proposed by Usov & Melrose 1995 who noticed that pairs are created then near the energy threshold, most favourably in bound states – as atoms of positronium – which then move to high altitudes before being ionized.

6. Radiative processes in pulsar magnetospheres

Cooling of ultrarelativistic electrons via curvature radiation (CR) and magnetic inverse Compton scattering (ICS) are the most natural ways of producing hard gamma-rays capable of inducing cascades of e^{\pm} -pairs and secondary HE photons. These two processes dominate within two distinct ranges of Lorentz factors γ of primary electrons.

When $\gamma \lesssim 10^6$, magnetic inverse Compton scattering plays a dominant role in braking the electrons and it is the main source of hard gamma-ray photons

(Sturmer et al. 1995). Energy losses due to resonant ICS limit the Lorentz factors of the particles to a level which depends on electric field strength \mathcal{E}_{\parallel} , temperature T and size of hot polar cap, and magnetic field strength B_s (Xia et al. 1985, Sturmer 1995). The Lorentz factors can then be limited even to $\sim 10^3$. This stopping effect becomes more efficient for stronger magnetic fields, and it was suggested as an explanation for the observed cutoff at $\sim 10\text{MeV}$ in the spectrum of B1509-58 (Sturmer 1995). ICS was also found to be able (under some circumstances) to smear out the monotonic energy distribution of electrons significantly, with interesting consequences for the cascades (Dyks & Rudak 2000b).

However, in their modern versions the accelerators of particles are strong enough to overpower the ICS cooling. In consequence, very high Lorentz factors – $\gamma \gtrsim 10^6$ – are achieved by electrons, limited by CR. The first detailed scenario of radiative processes in CR-induced cascades was presented by (Daugherty & Harding 1982) and despite many modifications and additions its basic features remain valid. The model assumes that primary electrons accelerated to ultrarelativistic energies emit curvature photons which in turn are absorbed by the magnetic field and e^{\pm} -pairs are created. These pairs cool off instantly via synchrotron radiation process. Whenever the SR photons are energetic enough they may lead to further creation of pairs, etc. ICS can still be incorporated to the models with CR-induced cascades as the process relevant for e^{\pm} -pairs, since typical Lorentz factors of theirs do not exceed $\sim 10^3$. According to the analytical model of Zhang & Harding 2000a the empirical relations for X-ray and gamma-ray luminosities of pulsars (presented in Sect.3) can be reproduced satisfactorily when the ICS involving e^{\pm} -pairs is included.

Processes relevant for generation and transfer of high-energy photons in pulsar magnetospheres are therefore:

- curvature radiation,
- magnetic inverse Compton scattering,
- magnetic pair creation ($\gamma \rightarrow e^{\pm}$)
- synchrotron radiation,
- photon splitting ($\gamma \rightarrow \gamma + \gamma$),
- photon-photon pair creation ($\gamma + \gamma \rightarrow e^{\pm}$).

Their basic properties are given below, except for $\gamma + \gamma \rightarrow e^{\pm}$: in practice it is treated exactly as in free space. This is justified in models of ‘thick outer gaps’ (Cheng & Zhang 1999) but within the framework of polar cap models this is not the case, in general. However, no handy formula is available for the cross section of this process in the limit of high B and standard non-magnetic formulae are in use (e.g. Zhang & Qiao 1998).

To illustrate how these processes contribute to the high-energy radiation of a pulsar the numerically calculated components (due to the first four processes in the list) are presented in Figs.4 and 5 (after Dyks & Rudak 2002a and Dyks et al. 2001) along with overlaid data points for the Vela pulsar. The dipolar

field in the Vela pulsar does not exceed 10^{13}G and photon splitting was neglected as non-competitive to the magnetic pair creation. The electric field structure of the accelerator used in these calculations is taken after Harding & Muslimov 1998a.

6.1. Curvature radiation

Relativistic electron of energy γmc^2 (we take $\gamma \gg 1$) sliding along the magnetic field line of curvature ϱ_{cr} will emit photons with a continuum energy spectrum peaked at the characteristic energy

$$\varepsilon_{\text{cr}} = \frac{3}{2} c \hbar \frac{\gamma^3}{\varrho_{\text{cr}}}. \tag{18}$$

The radius ϱ_{cr} for a purely dipolar line attached to the outer rim of the polar cap can be approximated not far away from the NS surface as $\varrho_{\text{cr}} \approx \sqrt{R_s \cdot R_{\text{lc}}} \approx 10^8 \sqrt{P} \text{cm}$. The cooling rate of that electron is

$$\dot{\gamma}_{\text{cr}} = -\frac{2}{3} \frac{e^2}{mc} \frac{\gamma^4}{\varrho_{\text{cr}}^2}. \tag{19}$$

For a monoenergetic injection function of electrons $Q(\gamma) \propto \delta(\gamma - \gamma_0)$ and their cooling due solely to CR the electrons will assume a single power-law distribution in energy space $N_{\gamma}(\text{el.}) \propto \gamma^{-4}$ for $\gamma < \gamma_0$ as long as they stay within the region of the cooling. Their escape introduces a natural low-energy cutoff γ_{cutoff} in $N_{\gamma}(\text{el.})$. Therefore, the unabsorbed CR energy spectrum $f_{\varepsilon}(\varepsilon)$ due to the injected electrons has a broken power-law shape, with a high-energy limit set by γ_0 and the break at some energy $\varepsilon_{\text{break}}$. For $\varepsilon > \varepsilon_{\text{break}}$ the energy spectrum is $f_{\varepsilon}(\varepsilon) \propto \varepsilon^{-2/3}$, and $f_{\varepsilon}(\varepsilon) \propto \varepsilon^{+1/3}$ for $\varepsilon < \varepsilon_{\text{break}}$. Since nonthermal spectra cover usually many decades in energy it is more convenient to use $\varepsilon f_{\varepsilon}(\varepsilon)$ for easy comparison of power in different parts of energy space (see Fig. 4). Accordingly, $\varepsilon f_{\varepsilon}(\varepsilon) \propto \varepsilon^{+1/3}$ above the break, and $\propto \varepsilon^{+4/3}$ below the break.

The cutoff limit γ_{cutoff} can be found by comparing the characteristic cooling time scale $t_{\text{cr}} \equiv \gamma/|\dot{\gamma}_{\text{cr}}|$ with the estimated time of escape t_{esc} , which we take as $t_{\text{esc}} \approx \varrho_{\text{cr}}/c$. Therefore

$$\varepsilon_{\text{break}} \approx \frac{9}{4} \hbar \frac{c}{r_0} \approx 150 \text{MeV}, \tag{20}$$

where r_0 is the classical electron radius (Rudak & Dyks 1999). Note, that photon energy $\varepsilon_{\text{break}}$ at which the cooling break occurs does not depend on any pulsar parameters.

The spectrum of CR calculated numerically to model the Vela pulsar (Dyks et al. 2001) is shown in Fig.4 as dot-dashed line. High-energy cutoff due to one-photon magnetic absorption occurs around 10 GeV. Note the importance of gamma-ray detectors capable to operate above 10 GeV for (in)validating the model. The low-energy CR spectral break $\varepsilon_{\text{break}}$ is prominent at $\sim 40\text{MeV}$. Below $\varepsilon_{\text{break}}$ the power of CR decreases and eventually becomes

unimportant at $\sim 1\text{MeV}$ where the synchrotron component takes over.

6.2. Magnetic pair creation

Pair creation via magnetic photon absorption ($\gamma + \mathbf{B} \rightarrow e^\pm + \mathbf{B}$) is kinematically correct because the magnetic field can absorb momentum. To ensure high chances for the process to occur it is not enough for a photon propagating at a pitch angle ψ to local \mathbf{B} to satisfy the energy threshold condition, $\sin\psi \cdot \varepsilon \geq 2mc^2$, but high optical thickness $\tau_{\gamma B}$ of the magnetosphere is required. In fact the condition $\tau_{\gamma B} = 1$ is used as a criterium for the so called death-line for radiopulsars in the $P - \dot{P}$ diagram. Maximal values of $\sin\psi$ for curvature photons in the dipolar field do not exceed $\sim 0.1 \sin\theta_{\text{pc}} \approx 0.0014 P^{-1/2}$ (Sturrock 1971), and, therefore, both conditions are difficult to be met for long-period pulsars.

The absorption coefficient for the process as described in Erber 1966 and used to calculate $\tau_{\gamma B}$ reads

$$\eta(\varepsilon) = \frac{1}{2} \frac{\alpha}{\lambda_c} \frac{B_\perp}{B_{\text{crit}}} T(\chi) \quad (21)$$

where α is a fine structure constant, λ_c is a Compton wavelength, $B_{\text{crit}} = m^2 c^3 / e \hbar \simeq 4.4 \times 10^{13} \text{G}$, B_\perp is the component of the magnetic field perpendicular to the photon momentum, and $\chi \equiv \frac{1}{2} \frac{B_\perp}{B_{\text{crit}}} \frac{\varepsilon}{m_e c^2}$ is the Erber parameter χ . The function $T(\chi)$ is then approximated as $T(\chi) \approx 0.46 \exp(-4f/3\chi)$, which is valid for $\chi \lesssim 0.2$; for $\chi \gtrsim 0.2$ this approximation starts to overestimate $\eta(\varepsilon)$ significantly. The function f is a near-threshold correction introduced by Daugherty & Harding 1983, important in the case of high local B . Electron-positron pairs created through the magnetic absorption emit synchrotron photons (SR) and also may get involved in ICS with soft photons.

Taking advantage of the dipolar character of the magnetic field, it is straightforward to find analytical approximation of the condition $\tau_{\gamma B} = 1$. A photon created at a radial distance r from the neutron star center, with its momentum parallel to the local magnetic field line will undergo magnetic absorption if its energy exceeds the following local cutoff energy (after Baring & Harding 2000, Baring 2001)

$$\varepsilon_{\text{cutoff}} \approx 0.4 P^{1/2} \left(\frac{r}{R_s} \right)^{1/2} \times \max \left\{ 1, \frac{0.1 B_{\text{crit}}}{B_{\text{pc}}} \left(\frac{r}{R_s} \right)^3 \right\} \text{GeV}. \quad (22)$$

This formula is valid for the magnetic field lines with their footpoints at the outer rim of the polar cap, of colatitude θ_{pc} (eq. 5), hence the dependence on \sqrt{P} . For other colatitudes θ the formula should be multiplied by $\theta_{\text{pc}}/\theta$.

6.3. Synchrotron radiation

Consider a particle of energy γmc^2 gyrating around a local field line at a pitch angle ψ . Let γ_\parallel denotes the Lorentz factor of the reference frame comoving with the center of the gyration. As long as $\gamma_\parallel \gg 1$ it relates to the pitch angle ψ via $\sin\psi \approx \gamma_\parallel^{-1}$. The energy available for synchrotron emission at the expense of the particle is $\gamma_\perp mc^2$, and $\gamma = \gamma_\perp \gamma_\parallel$.

The rate of SR cooling reads

$$\dot{\gamma}_{\text{sr}} = -\frac{2}{3} \frac{r_0^2}{m_e c} B^2 \gamma_\perp^2 = -\frac{2}{3} \frac{r_0^2}{m_e c} B^2 \sin^2\psi \gamma^2. \quad (23)$$

In comparison to the CR cooling it is enormous (due to much smaller curvature radius).

Critical photon energy (analogous to (18)) reads

$$\varepsilon_{\text{sr}} = \frac{3}{2} \hbar \frac{eB}{m_e c} \gamma^2 \sin\psi. \quad (24)$$

For a monoenergetic injection function of particles (e^\pm -pairs in the context of this review) and their cooling due to SR the energy spectrum of SR spreads between a high-energy limit $\varepsilon_{\text{sr}}(\gamma_0)$ set by γ_0 of the injected (created) particles, and a low-energy turnover ε_{ct} determined by the condition $\gamma_\perp \sim 1$:

$$\varepsilon_{\text{ct}} \equiv \varepsilon_{\text{sr}}(\gamma = \gamma_\parallel) = \frac{3}{2} \hbar \frac{eB}{m_e c} \frac{1}{\sin\psi}. \quad (25)$$

The spectrum assumes a single power-law shape $f_\varepsilon(\varepsilon) \propto \varepsilon^{-1/2}$ (and accordingly $-\varepsilon f_\varepsilon(\varepsilon) \propto \varepsilon^{+1/2}$) above the turnover. Below ε_{ct} , the spectrum f_ε changes its slope, asymptotically reaching $\propto \varepsilon^{+2}$. It is built up by contributions from low-energy tails emitted by particles with $\gamma_\perp \gg 1$, and each low-energy tail cuts off at local gyrofrequency, which in the reference frame comoving with the center of gyration is $\omega_B = \frac{eB}{m_e c \gamma_\perp}$. The spectrum of SR calculated with Monte-Carlo method to model the Vela pulsar is shown in Fig.4 as a dashed line. The low-energy part of the SR spectrum at ε_{ct} seems to be essential for connecting the RXTE and the OSSE points.

Synchrotron as well as cyclotron emission become prohibited at strong local magnetic fields $B \gtrsim 0.1 B_{\text{crit}}$ (Usov & Melrose 1995, Arendt & Eilek 2001) – the magnetic photon absorption proceeds here close to the threshold, and the pairs created do not occupy excited Landau levels. In consequence, electromagnetic cascades are expected to be notably weaker than for $B < 0.1 B_{\text{crit}}$. Along with photon splitting (Baring & Harding 2001), this may explain why do radiopulsars avoid the high-B region in the $P - \dot{P}$ diagram.

6.4. Magnetic Inverse Compton Scattering

Consider an electron with a Lorentz factor γ moving along a magnetic field line \mathbf{B} and a photon of energy $\varepsilon = \epsilon mc^2$ moving at angle μ to the field line. In the reference

frame comoving with the electron (primed symbols) the counterpart of the free-space Compton formula, due to energy-momentum conservation appropriate for collisions with the electron at the ground Landau level both in the initial and final state, reads

$$\epsilon'_s = \left(1 - \mu_s'^2\right)^{-1} \left\{ 1 + \epsilon'(1 - \mu'\mu'_s) + \right. \\ \left. - \left[1 + 2\epsilon'\mu'_s(\mu'_s - \mu') + \epsilon'^2(\mu'_s - \mu')^2 \right]^{1/2} \right\} \quad (26)$$

where $\epsilon' = \epsilon\gamma(1 - \beta\mu)$ (Herold 1997), and symbols with no subscript and with the subscript ‘s’ refer to the state before the scattering and after the scattering, respectively. A longitudinal momentum of the electron in the electron rest frame changes due to recoil from zero to $(\epsilon'\mu' - \epsilon'_s\mu'_s)mc$.

The polarization-averaged relativistic magnetic cross section in the Thomson regime may be approximated with a nonrelativistic formula (Dermer 1990):

$$\sigma = \frac{\sigma_T}{2} \left(1 - \mu'^2 + (1 + \mu'^2) \left[g_1 + \frac{g_2 - g_1}{2} \right] \right) \quad (27)$$

where σ_T is the Thomson cross section, and g_1 and g_2 are given by

$$g_1(u) = \frac{u^2}{(u+1)^2}, \quad g_2(u) = \frac{u^2}{(u-1)^2 + a^2} \quad (28)$$

where $u \equiv \epsilon'/\epsilon_B$, $a \equiv 2\alpha\epsilon_B/3$, $\epsilon_B \equiv \hbar eB/m^2c^3$ and α is a fine-structure constant. The resonance condition for the scattering is therefore the cyclotron resonance $\epsilon' = \epsilon_B$. The factor a represents a ‘natural’ broadening of the resonance due to finite lifetime at the excited Landau level.

In the Klein-Nishina regime ($\epsilon' > 1$) the relativistic magnetic cross section for the $|\mu'| \approx 1$ case becomes better approximated with the well known Klein-Nishina relativistic nonmagnetic total cross section σ_{KN} (Daugherty & Harding 1986, Dermer 1990).

The rate \mathcal{R} of scatterings subject by an electron moving across the field of soft photons, measured in the lab frame is

$$\mathcal{R} = c \int d\Omega \int d\epsilon \sigma \left(\frac{dn_{\text{ph}}}{d\epsilon d\Omega} \right) (1 - \beta\mu) \quad (29)$$

where $\Omega = d\mu d\phi$ is the total solid angle subtended by the source of soft photons, $\mu = \cos\theta$, σ is a total cross section for the process, and $dn_{\text{ph}}/d\epsilon/d\Omega$ is the local density of the soft photons.

The properties of the field of soft photons are usually simplified by taking $dn_{\text{ph}}/d\epsilon/d\Omega$ as for the blackbody radiation. This simplification should be taken with care since magnetised atmospheres of neutron stars introduce strong anisotropy as well as spectral distortions to the outgoing radiation (Pavlov et al. 1994). Effectively it means that the ICS effects obtained with this simplification are just upper limits to the actual effects.

To estimate electron cooling rate $\dot{\gamma}_{\text{ICS}}$ due to the ICS the differential form of (27) is necessary:

$$\frac{d\sigma}{d\Omega'_s} = \frac{3\sigma_T}{16\pi} \left[(1 - \mu'^2)(1 - \mu_s'^2) + \right. \\ \left. + \frac{1}{4} (1 + \mu'^2)(1 + \mu_s'^2)(g_1 + g_2) \right] \quad (30)$$

(eg. Daugherty & Harding 1989), where $d\Omega'_s = d\phi'_s d\mu'_s$ is an increment of solid angle into which outgoing photons with energy ϵ'_s in the electron rest frame are directed. The mean electron energy loss rate then reads

$$\dot{\gamma}_{\text{ICS}} = -c \int d\epsilon \int d\Omega \left(\frac{dn_{\text{ph}}}{d\epsilon d\Omega} \right) (1 - \beta\mu) \times \\ \times \int d\Omega'_s \left(\frac{d\sigma}{d\Omega'_s} \right) (\epsilon_s - \epsilon) \quad (31)$$

where $\epsilon_s = \epsilon'_s\gamma(1 + \beta\mu'_s)$ is the scattered photon energy in the lab frame (e.g. Dermer 1990).

The spectrum of magnetic ICS calculated numerically to model the Vela pulsar is shown in Figs.4 and 5 with thin solid line. The blackbody soft photons originating at the stellar surface (dotted line) are upscattered by secondary e^\pm -pairs at the expense of their ‘‘longitudinal’’ energy $\gamma_{\parallel}mc^2$, assumed to remain unchanged during the burst of synchrotron emission. Without the ICS component due to the e^\pm -pairs the RXTE data for the Vela pulsar would be difficult to reproduce within the model. It is worth to note, that the magnetic ICS component due to primary electrons (not shown in Fig.4) is energetically insignificant comparing to the CR component.

6.5. Photon splitting

Photon splitting into two photons in the presence of magnetic field B is a third-order QED process with no energy threshold (Adler 1971). The attenuation coefficient, after averaging over the polarization states, reads (Harding et al. 1997)

$$T_{\text{split}}(\epsilon) \approx \frac{\alpha^3}{10\pi^2} \frac{1}{\lambda_c} \left(\frac{19}{315} \right)^2 \left(\frac{B \sin\theta_{\text{KB}}}{B_{\text{crit}}} \right)^6 \epsilon^5 \text{ cm}^{-1}, \quad (32)$$

(provided B does not exceed B_{crit} substantially) where α is a fine structure constant, ϵ is the photon energy in units of mc^2 , θ_{KB} is the angle between photon momentum vector and the local magnetic field. The process, therefore, strongly depends on magnetic field strength B .

Photon splitting has attracted substantial interest in recent years due to the discovery of neutron stars with supercritical magnetic fields (Mereghetti 1999). It has been analysed in details by Harding et al. 1997 and incorporated in a Monte Carlo code tracing the propagation of electromagnetic cascades in the magnetospheres of high- B pulsars. The effect was found to explain satisfactorily the unusual cut-off observed in the gamma-ray spectrum of B1509-58 (see Sect.3). Generally, it becomes competitive

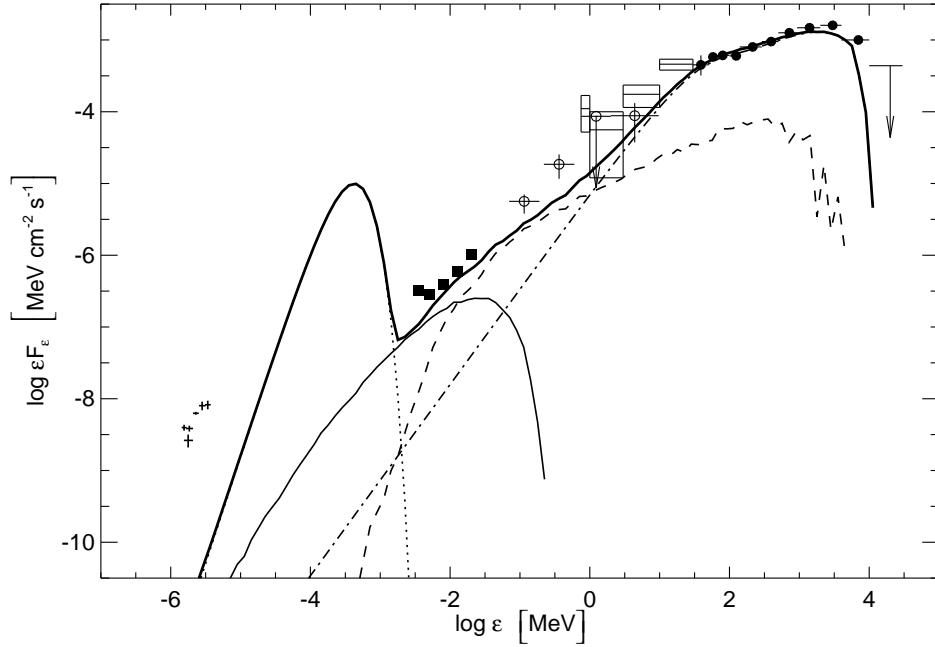


Fig. 4. The model energy spectrum calculated by Dyks & Rudak 2002a to reproduce the spectral features of the Vela pulsar ($P = 89$ ms, $B_s = 6 \times 10^{12}$ G). The accelerator is located at $h_0 = 3R_s$ above the surface (see Sect.6). The broad-band spectrum consists of four components due to: curvature radiation of primary electrons (dot-dashed), synchrotron radiation of secondary e^\pm -pairs (dashed), inverse Compton scattering of surface X-ray photons on the e^\pm -pairs (thin solid) and the blackbody surface emission (dotted). The surface temperature $T_s = 1.26 \times 10^6$ K was assumed for the neutron star. Total spectrum is given by a thick solid line. Phase-averaged data points for Vela from different telescopes are indicated: crosses – multicolor photometry with NTT and HST (Mignani & Caraveo 2001); filled squares – RXTE (Strickman et al. 1999); open circles – OSSE (Strickman et al. 1996); rectangles – COMPTEL (Schönfelder et al. 2000); filled circles plus an upper limit just above 10 GeV – EGRET (Thompson et al. 1997).

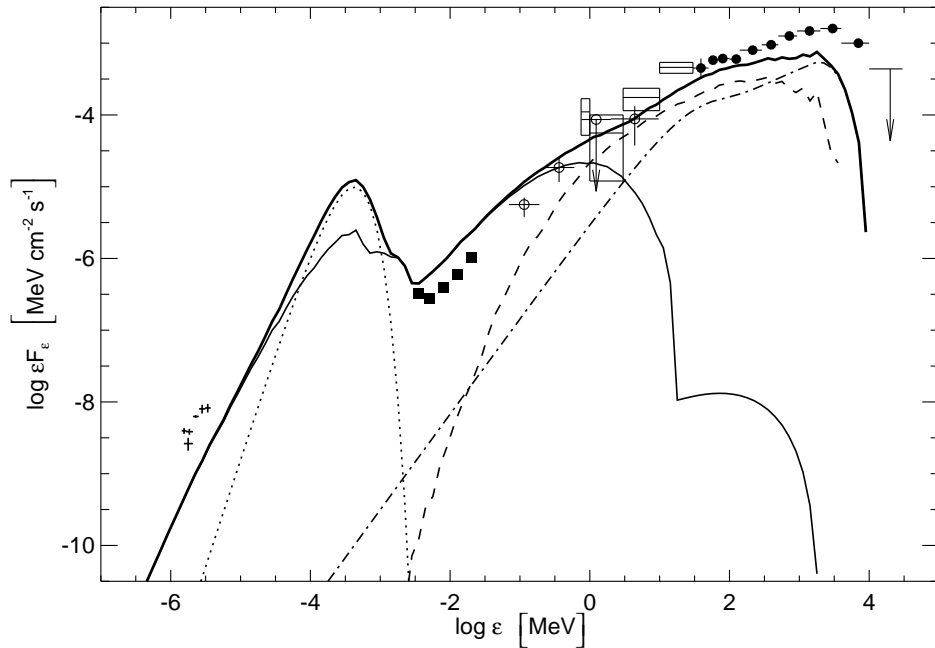


Fig. 5. Same as Fig. 4 but with two parameters changed drastically ($B_s = 0.6 \times 10^{12}$ G, $h_0 = 0$) in order to obtain as much power in the optical range as possible by modifying the ICS component due to e^\pm -pairs (thin solid line). Despite unrealistically favourable conditions to down-scatter some of the blackbody photons, the low-energy tail of the ICS component falls short by a factor of ~ 3 below the observed optical flux level (crosses).

to the magnetic pair creation for dipolar magnetospheres with $B_s \gtrsim 0.3B_{\text{crit}}$ (Harding et al. 1997). The degradation of photon energy in the course of splitting inhibits also any development electromagnetic cascades. In consequence, high- B RPP should not emit coherent radio emission. Indeed, there exists a high- B region in the $P - \dot{P}$ diagram void of radiopulsars. Even though three recently discovered (during The Parkes Multibeam Pulsar survey) high- B radiopulsars (Camilo et al. 2000) are located above the formal limiting line derived in Baring & Harding 1998 (and elaborated in Baring & Harding 2001), the general argument that magnetars are expected to be radio-quiet RPP remains valid (Zhang & Harding 2000b).

7. Facing the Vela pulsar

In order to fit our model to the phase averaged spectrum of Vela over almost 8 decades in energy (see Fig.4) we were forced to locate the accelerator at the altitude of $h_0 \simeq 3R_s$, i.e. unrealistically high for any version of polar-cap models. The same problem was encountered by Daugherty & Harding 1996 when modelling the CGRO data points of Vela.

Physical justification for lifting the accelerator up to $\sim 1R_s$ might rely on a mechanism proposed by Harding & Muslimov 1998a. They considered a sandwich-like structure of two pair formation fronts (PFF), controlled by either CR or ICS, where the lower PFF would be formed due to positrons returning from the upper PFF. With reasonable surface temperatures ($T_s \sim 5 \times 10^5 \text{K}$) it is ICS which dominates (comparing to CR) in generating high-energy quanta at the energetic expense of upward moving electrons and downward moving positrons. Such a situation is not symmetrical and not stable, therefore. Accordingly, the lower PFF tends to elevate until the CR-cooling takes over, which happens at $h_0 \sim 1R_s$. Unfortunately, this mechanism – rather promising in the context of required $h_0 \simeq 3R_s$, even though $3R_s$ is still notably more than $\sim 1R_s$ – has been invalidated by recent numerical calculations: Harding & Muslimov 2002 concluded the inability of ICS-controlled upper PFFs to develop lower PFFs because of too low multiplicities in such cases.

The requirement of high-altitude accelerator for Vela is likely to be extended to other gamma-ray pulsars. A piece of hint for such a requirement comes from a strong correlation for known gamma-ray pulsars between the inferred magnetic field strength and the value of high-energy cutoff (Baring & Harding 2000). [Note, that this empirical correlation speaks in favor of high-energy cutoffs in pulsar spectra originating due to magnetic absorption of gamma-rays – a signature of polar-cap models.] This is shown in Fig.6 along with the dependence of $\varepsilon_{\text{cutoff}}$ on the location of photon emission point r according to eq.(22).

Last but not least – a real challenge for all contemporary models for Vela comes from the phase-resolved spectral analysis of pulsed hard X-rays and the phasing of

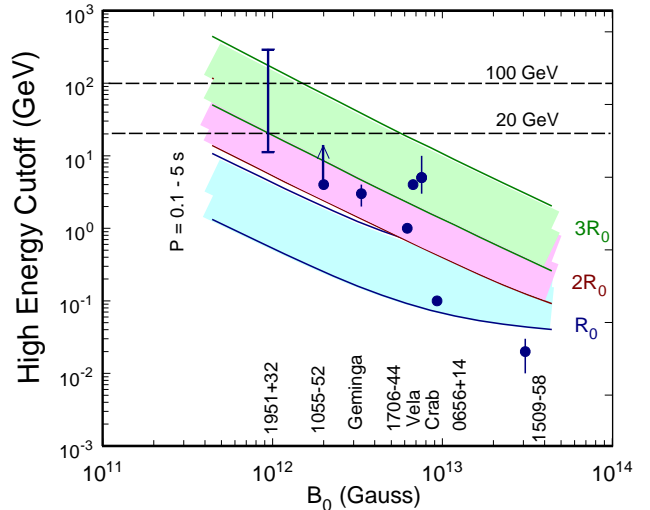


Fig. 6. Spectral cutoff energies estimated for eight gamma-ray pulsars are plotted against inferred surface magnetic field strengths B_s . Three shaded bands (note the overlaps) indicate the location of $\varepsilon_{\text{cutoff}}$ according to eq.(22) for three values of the emission altitude ($r = R_s, 2R_s$ and $3R_s$) and for the range of spin periods P between 0.1 and 5 s. (From Baring & Harding 2000 and Baring 2001; courtesy of Matthew Baring.)

the lightcurves in optical, X-rays and gamma-rays, presented by Strickman et al. 2001 and Harding et al. 2002. The strong double-peak lightcurve in optical (fig.1 in these refs.) is particularly enigmatic. The peak-to-peak separation is notably smaller than in HE domain. Moreover, the leading peak has no counterpart in any other energy range (including the radio). The trailing optical peak seems to be associated with the trailing RXTE peak and with the trailing gamma-ray peak, though the latter lags behind the trailing optical by about 0.1 in phase. Extrapolation of the gamma-ray spectrum taken for either of the two gamma-ray peaks falls below the phase-averaged optical flux level (by a factor ~ 10 in the case of the trailing gamma-ray peak).

The problem of optical emission is also difficult to solve in the framework of our phase-averaged approach to model the spectrum of Vela. A difficult task we have faced was to find a component (without referring to any ingredients external to the model) that would account for the optical emission, at least in some particular circumstances. Fig.5 gives an example of what can be achieved at best in the optical domain of the model spectrum, but at the price paid at the high-energy end of the spectrum.

8. Millisecond pulsars

The question of whether millisecond pulsars (i.e. with low magnetic fields) do emit gamma-rays will be hopefully answered within the next five years with GLAST. On theoretical side, there had been some attempts to address this

problem. For instance, Wei et al. 1996 presented broad-band spectra of both pulsed and unpulsed emission expected in their version of the outer-gap model. In the framework of polar-cap scenarios, Sturmer & Dermer 1994 made their predictions for gamma-ray luminosity L_γ by scaling down with B their analytical formulae for L_γ for classical pulsars. Rudak & Dyks 1998 proposed a modification of the model by Daugherty & Harding 1982; this modification incorporates a contribution of electron-positron pairs to L_γ , which becomes a non-monotonic function of B (see Figs. 7 and 8 of Dyks 1998). One of the consequences of this modification is that expected values of L_γ for millisecond pulsars, including J0437-4715, are typically about one or two orders of magnitude lower than for classical pulsars (see Fig.3 in section 3). Quantitatively similar estimate, though for a different reason, comes from the model of Dermer & Sturmer 1994. If these estimates are correct then some millisecond pulsars, including J0437-4715 (see Fig.7), should be detected with next-generation experiments, providing thus a testing ground for magnetospheric models relevant for millisecond pulsars. GLAST is expected to have sensitivity above 100MeV about 30 times higher than EGRET, and it will reach high-energy limit at 300GeV - closing thus for the first time the energy gap between the VHE (very high energy) domain accessible with ground-based Cherenkov techniques and the HE (high energy) domain of satellite experiments (Kamae et al. 2000). Moreover, millisecond pulsars are expected to radiate mostly in the range between 10GeV and 100GeV, this class of objects should be of interest for the upcoming IAC telescope MAGIC (Blanch et al. 1998).

For the time being, the only millisecond pulsar marginally detected above 100 MeV (at 3.5σ level) is PSR J0218+4232, with the spin period $P = 2.3$ ms and the inferred magnetic field $B_{pc} \simeq 8.6 \times 10^8$ G, (Verbunt et al. 1996). The inferred luminosity of the pulsed emission for 1 steradian opening angle reaches $L_\gamma \simeq 1.64 \times 10^{34} \text{erg s}^{-1} \simeq 0.07 L_{sd}$. Broad-band spectrum of this pulsar differs from the HE spectra known for young gamma-ray pulsars: above 100 MeV the photon index $\alpha_{ph} \sim -2.6$ (Kuiper et al. 2000) and the spectrum resembles soft spectra of EGRET UID sources; within the BeppoSAX range the spectrum is extremely hard, with $\alpha_{ph} \simeq -0.61 \pm 0.32$ (Mineo et al. 2000). Off-beam geometry (i.e. the line of sight misses the hollow cone beam) was recently proposed (Dyks & Rudak 2002) for this pulsar. In such a situation the high energy ‘‘cutoff’’ occurs at a relatively low energy ~ 100 MeV (marked by two EGRET points, see Fig.8). Unlike in on-beam cases, this cutoff is not due to magnetic absorption; it corresponds to a maximum energy of those electrons which emit curvature photons towards the observer. The shape of the apparent cut-off can easily mimic very soft spectra (Harding & Zhang 2001 used similar viewing geometry arguments to explain very soft spectra of EGRET

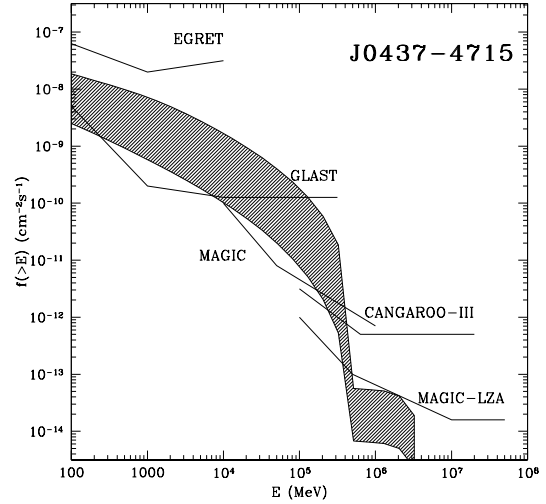


Fig. 7. Cumulative spectral flux of photons expected for the millisecond pulsar J0437-4715 at a distance of 140 pc. The shaded region shows the range of flux levels due to uncertainty in the maximal energy of primary electrons. The main part of the spectrum is due to curvature radiation of the electrons. The additional feature reaching the VHE domain is due to inverse Compton scattering of soft photons from the surface with the temperature 4×10^5 K. Sensitivities of EGRET as well as three major HE and VHE experiments of the future are indicated. MAGIC-LZA denotes sensitivity of MAGIC in its Large Zenith Angle mode. (After Bulik et al. 2000).

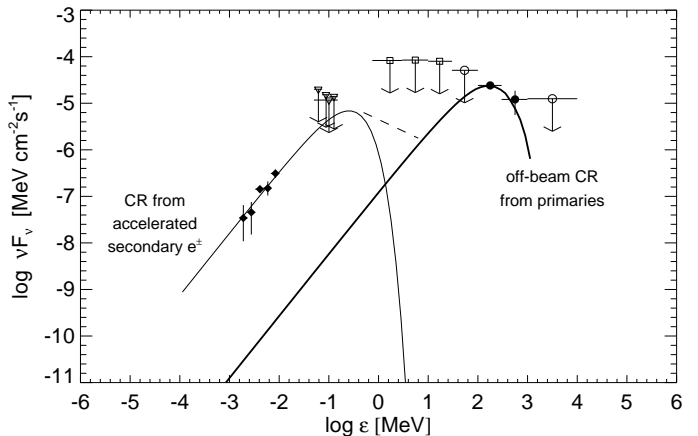


Fig. 8. Two-component theoretical spectrum for the off-beam geometry (continuous lines) is compared with the spectrum observed for PSR J0218+4232 (diamonds – BeppoSAX, triangles – OSSE, squares – COMPTEL, circles – EGRET). The low energy component is due to curvature radiation from secondary e^\pm pairs (with energy $\sim 10^5$ MeV acquired upon their acceleration in a residual electric field), whereas the high-energy component is due to curvature radiation from primary electrons (with energy $\sim 10^7$ MeV). (From Dyks & Rudak 2002.)

UID sources). The BeppoSAX points are explained in this model as due to curvature radiation of secondary e^\pm pairs accelerated within the polar gap. Upon the acceleration in a residual electric field, the e^\pm pairs should reach the energy γ_{\parallel} between 1.5×10^5 and 6×10^5 , which is about 1% of the primary electron energy. A few hundred of pairs per primary electron are required to be accelerated in order to reproduce the BeppoSAX level. According to Harding & Muslimov 2001 and 2002, acceleration of such a large number of pairs within the polar gap is difficult to achieve.

9. Viewing geometry effects

Viewing geometry has been recognized as an important factor in shaping the lightcurves as well as broadband energy spectra of particular objects (like e.g. the Vela pulsar, see Harding & Muslimov 1998) as well as in the context of EGRET UID galactic sources (e.g. recent review by Baring 2001).

To taste a variety of apparent pulsar characteristics accessible upon changing the viewing angle ζ we present here two cases: of a classical pulsar in Fig.9 and a millisecond pulsar in Fig.10. The lightcurves (these are energy-integrated above 100 MeV) and the gamma-ray spectra were calculated with our numerical code. The spectra are two-component: due to curvature and synchrotron emission; inverse Compton scattering was neglected. The effects of aberration and light travel delays were included. These effects are important for millisecond pulsars, and affect their lightcurves, especially at large inclination angles α (the case not shown here). Whenever the line of sight misses outer rim of the polar cap, the observed spectra become soft with an apparent exponential (and not super-exponential) decay, mimicking thus an outer-gap candidate. The millisecond gamma-ray pulsar J0218+4232 (Fig.8) is probably a good example of such a case.

10. Concluding remarks

High-energy astrophysics of pulsars was challenged by unexpected richness of spectral and temporal properties found for the brightest gamma-ray pulsars. Numerous modifications (both, minor and major) to the existing models of magnetospheric activity are being invented to accommodate at least some of these properties. It is clear, however, that we actually need good quality high-energy data for much weaker sources. Only then it will be possible to assess on statistical grounds the significance of those properties (the argument used by many authors, recently reiterated strongly by Baring 2001). Chances are that it may have happen in a few years time.

The planned observatory GLAST (Kamae et al. 2000) will be superior to EGRET in two aspects. First, its sensitivity at 10 GeV will be more than two orders of magnitude better than that of EGRET. Second, it will reach

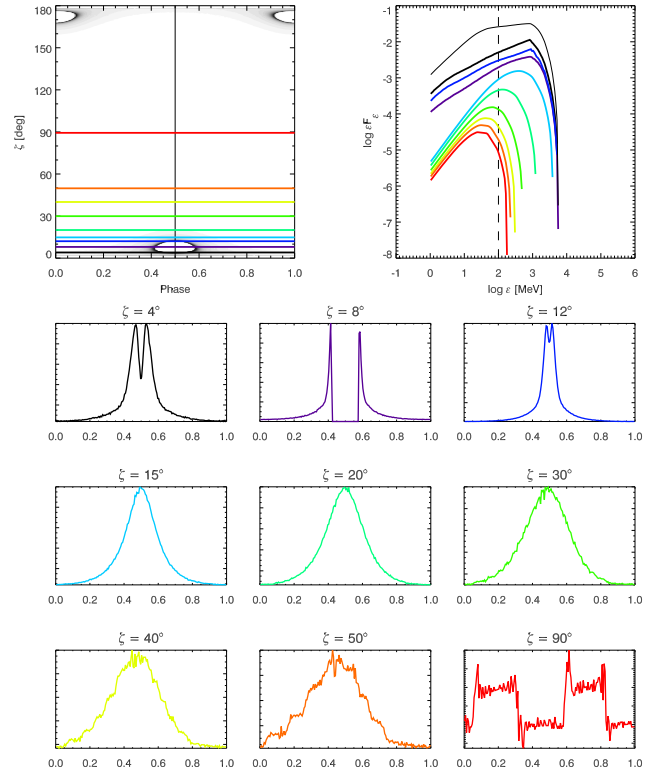


Fig. 9. The characteristics of high energy radiation expected from a classical pulsar with $P = 0.1$ s, $B = 10^{12}$ G and the magnetic dipole inclination $\alpha = 8^\circ$. The top left panel shows the intensity distribution for radiation above 100 MeV as a function of rotational phase ϕ and viewing angle ζ . Horizontal color-coded lines correspond to the position of nine observers located at different angles ζ . For each ζ the phase-averaged spectrum drawn with color-coded line is shown in top right panel. The corresponding pulse profiles are shown in small panels labelled with ζ . The spectrum of total luminosity from the pulsar (thin solid line in top right panel) is plotted (at an arbitrary level relative to the phase-averaged spectra) for comparison of the shapes. (From Woźna et al. 2002).

energy of 300 GeV, closing thus for the first time the energy gap between satellite and ground-based observatories (HE and VHE, respectively). The MAGIC Telescope (Blanch et al. 1998) – a 17 m diameter Imaging Air Cherenkov Telescope (IACT) – is expected to operate with sensitivity about three orders of magnitude higher at 10 GeV than EGRET. Its advanced technology will make possible to cover energy range between 10 GeV and 1 TeV, and to reach ~ 50 TeV in the Large Zenith Angle mode. Energy ranges of GLAST and MAGIC will overlap over more than one decade in energy.

We expect that the question of whether millisecond pulsars emit gamma-rays at all, will be answered relatively

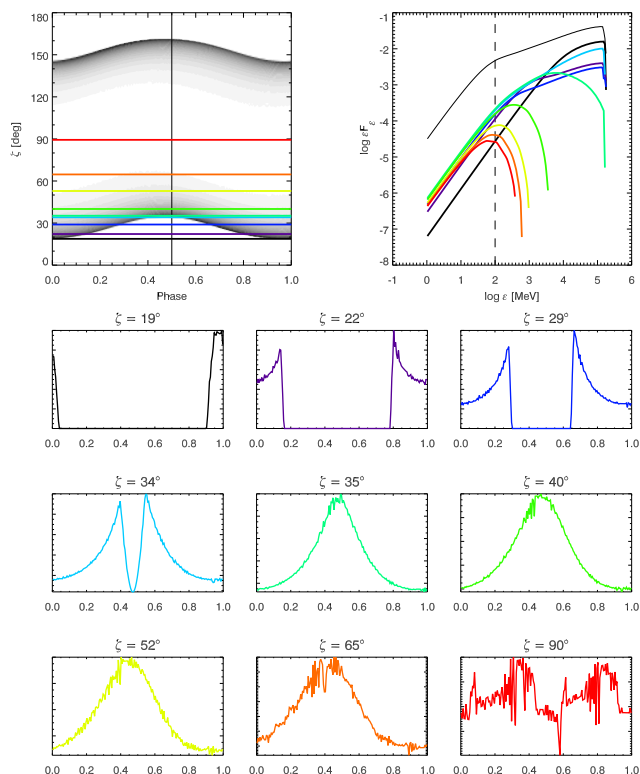


Fig. 10. Same as fig.9, but for a millisecond pulsar with $P = 2.3$ ms, $B = 10^9$ G and different set of viewing angles ζ . (From Woźna et al. 2002).

easily with these high-sensitivity observatories, verifying at first the status of J0218+4232.

In the context of numerous positive detections anticipated at hard gamma-rays, inclusion of viewing geometry effects will be of particular importance to properly interpret the observed shapes of spectral turnovers at high-energy ends.

To tackle high-quality data of the future in the most effective way, numerical 3D codes should be developed, capable of fast tracing the development and propagation of electromagnetic cascades in variety of non-dipolar realizations of magnetic field structure. Relaxing the centered-dipole assumption as a first step would be very much in line with recent conclusions from the soft X-ray data analysis for neutron stars (Pavlov et al. 2002). Optical to gamma-ray properties of Vela (section 7) are in our opinion a signature of a strongly non-axisymmetric hollow cone of radiation around the magnetic axis. Strong deviations of the actual magnetic field structure from a pure dipole at the stellar surface may well be responsible for inducing this axial asymmetry already at the site of electron acceleration. (Recently, multipolar character of open field lines has been considered in a quantitative way by Gil et al. 2002 to justify radiopulsars with vacuum gap solutions in pulsars with superstrong magnetic fields.) An

advantage of incorporating multipolar components to the polar-cap models is twofold:

- 1) magnetic field strength may locally be lowered slightly, opening thus windows for GeV photons to escape without magnetic attenuation; postulating high-altitude accelerators would be then unnecessary.
- 2) directional characteristics of high-energy radiation would change notably with respect to the dipolar axis at higher altitudes, where radio emission is generated.

Acknowledgements. BR acknowledges financial support by Wilhelm und Else Heraeus-Stiftung; he also wishes to thank the organizers of the Bad-Honnef Seminar for invitation and warm hospitality. This work was supported by the KBN grants: 2P03D02117 (BR, TB) and 5P03D02420 (JD).

References

- Adler, S.L., 1971, *Ann.Phys.*, 67, 599
- Arendt, P.N., Jr., Eilek, J.A., 2000, In: *IAU Coll. 177, Pulsar Astronomy - 2000 and Beyond* ed. M. Kramer, N. Wex, R. Wielebinski (ASP Conference Series, 202, 445)
- Arons, J., 2000, In: *IAU Coll. 177, Pulsar Astronomy - 2000 and Beyond* ed. M. Kramer, N. Wex, R. Wielebinski (ASP Conference Series, 202, 449)
- Arons, J. & Scharlemann, E.T., 1979, *ApJ*, 231, 854
- Baring, M.G., 2001, *Proc. Tonantzintla Workshop*, eds. A. Carramiñana et al. (Kluwer Academic, Dordrecht), astro-ph/0106161
- Baring, M.G. & Harding, A.K., 1998, *ApJ*, 507, L55
- Baring, M.G. & Harding, A.K., 2000, *Bull. AAS*, 32, 12.43
- Baring, M.G. & Harding, A.K., 2001, *ApJ*, 547, 929
- Becker, W., 2002, this proceedings
- Becker, W. & Truemper, J., 1997, *A&A*, 326, 682
- Becker, W. & Truemper, J., 1999, *A&A*, 341, 803
- Beskin, V.S., 1990, *Sov. Astron. Lett.*, 16(4), 286
- Blanch, O. et al., 1998, 'The MAGIC telescope', Letter of Intent
- Bulik, T., Rudak, B., Dyks, J., 2000, *MNRAS*, 317, 97
- Camilo, F. et al., 2000, *ApJ*, 541, 367
- Chen, K. & Ruderman, M., 1993, *ApJ*, 402, 264
- Cheng, K.S. & Zhang, L., 1999, *Fundamentals of Cosmic Physics*, 20, 177
- Cheng, K.S., Ho, C., Ruderman, M.A., 1986, *ApJ*, 300, 500
- Cheng, K.S., Ho, C., Ruderman, M.A., 1986, *ApJ*, 300, 522
- Daugherty, J.K. & Harding, A.K., 1982, *ApJ*, 252, 337
- Daugherty, J.K. & Harding, A.K., 1983, *ApJ*, 273, 761
- Daugherty, J.K. & Harding, A.K., 1986, *ApJ*, 309, 362
- Daugherty, J.K. & Harding, A.K., 1989, *ApJ*, 336, 861
- Daugherty, J.K. & Harding, A.K., 1994, *ApJ*, 42, 325
- Daugherty, J.K. & Harding, A.K., 1996, *ApJ*, 458, 278
- Dermer, C.D., 1990, *ApJ*, 360, 197
- Dermer, C.D. & Sturmer, S.J., 1994, *ApJ*, 420, L75
- Dyks, J., 1998, *Acta Astron.*, 48, 355
- Dyks, J. & Rudak, B., 2000a, *A&A*, 362, 1004
- Dyks, J. & Rudak, B., 2000b, *A&A*, 360, 263
- Dyks, J. & Rudak, B., 2000c, *MNRAS*, 319, 477
- Dyks, J. & Rudak, B., 2002, *XXII Ind Moriond Meeting 'The Gamma-Ray Universe'*, in press (astro-ph/0205222)
- Dyks, J. & Rudak, B., 2002a, in preparation

- Dyks, J., Rudak, B., Bulik, T., 2001, Proc. of the 4th INTEGRAL Workshop, ESA SP, 459, 191,
- Erber, T., 1966, Rev.Mod.Phys., 38, 626
- Fierro, J.M. et al., 1995, ApJ, 447, 807
- Gil, J., Melikidze, G.I., Mitra, D., 2002, A&A, 388, 235
- Goldreich, P. & Julian, W.H., 1969, ApJ, 157, 869
- Gotthelf, E.V. et al., 2000, ApJ, 542, L37
- Halpern, J.P. & Wang, F.Y.-H., 1997, ApJ, 477, 905
- Harding, A.K., Baring, M.G., Gonthier, P.L., 1997, ApJ, 476, 246
- Harding, A.K., Contopoulos, I., Kazanas, D., 1999, ApJ, 525, L125
- Harding, A.K. et al., 2002, ApJ, in press (astro-ph/0205183)
- Harding, A.K. & Muslimov, A.G., 1998, ApJ, 500, 862
- Harding, A.K. & Muslimov, A.G., 1998a, ApJ, 508, 328
- Harding, A.K. & Muslimov, A.G., 2001, ApJ, 556, 987
- Harding, A.K. & Muslimov, A.G., 2002, ApJ, 568, 862
- Harding, A.K. & Zhang, B., 2001, ApJ, 548, L37
- Herold, H., 1979, Phys.Rev.D, 19, 2868
- Jessner, A., Lesch, H., Kunzl, T., 2001, ApJ, 547, 959
- Kamae, T. et al., 2000, Adv.Sp.Res., 25, 905
- Kanbach, G., 2002, this proceedings
- Kluźniak, W. & Rudak, B., 1996, unpublished
- Kuiper, L. et al., 1999, A&A, 351, 119
- Kuiper, L. et al., 2000, A&A, 359, 615
- Marshall, F.E. et al., 1998, ApJ, 499L, 179
- Mereghetti, S., 1999, In: *NATO ASI The Neutron Star - Black Hole Connection*
- Michel, F.C., 1974, ApJ, 192, 713
- Michel, F.C., 1991, *Theory of Neutron Star Magnetospheres* (The University of Chicago Press, Chicago)
- Mignani, R.P. & Caraveo, P.A., 2001, A&A, 376, 213
- Mineo, T. et al., 2000, A&A, 355, 1053,
- Muslimov, A.G. & Tsygan, A.I., 1992, MNRAS, 255, 61
- Nel, H.I. et al., 1996, ApJ, 465, 898
- Pavlov, G.G. et al., 1994, A&A, 289, 837
- Pavlov, G.G. et al., 2002, this proceedings
- Rudak, B. & Dyks, J., 1998, MNRAS, 295, 337
- Rudak, B. & Dyks, J., 1999, MNRAS, 303, 477
- Ruderman, M.A. & Sutherland, P.G., 1975, ApJ, 196, 51
- Saito, Y. et al., 1997, ApJ, 477, L37
- Saito, Y. et al., 1998, In: *Neutron Stars and Pulsars: Thirty Years after the Discovery* ed. N. Shibasaki, et al. (Universal Academy Press: Tokyo) pp.295-298
- Sako, T. et al., 2000, ApJ, 537, 422
- Schönfelder, V. et al., 2000, A&AS, 143, 145
- Schroeder, P.C. et al., 1995, ApJ, 450, 784
- Strickman, M.S. et al., 1996, ApJ, 460, 735
- Strickman, M.S., Harding, A.K., de Jager, O.C., 1999, ApJ, 524, 373
- Strickman, M.S. et al., 2001, In: *Gamma-Ray Astrophysics 2001* ed. S. Ritz et al. (AIP), 570
- Sturmer, S.J., 1995, ApJ, 446, 292
- Sturmer, S.J. & Dermer, C.D., 1994, A&A, 281, L101
- Sturmer, S.J., Dermer, C.D., Michel, F.C., 1995, ApJ, 445, 736
- Sturrock, P.A., 1971, ApJ, 164, 529
- Takahashi, M. et al., 2000, In: *IAU Coll. 177, Pulsar Astronomy - 2000 and beyond* ed. M. Kramer, N. Wex, R. Wielebinski (ASP Conference Series, 202: 2000) pp.353-354
- Taylor, J.H. et al., 1995, 'The Princeton Pulsar Database' (<http://pulsar.princeton.edu>)
- Thompson, D.J., 2001, In: *International Symposium on High Energy Gamma-Ray Astronomy*, ed. F. A. Aharonian, & H. J. Völk, AIP Conference Proceedings, vol. 558, 103
- Thompson, D.J. et al., 1997, In: *Fourth Compton Symposium* ed. by C.D. Dermer, M.S. Strickman, J.D. Kurfess (New York: AIP 1997) 410
- Thompson, D.J. et al., 1999, ApJ, 516, 297
- Usov, V.V. & Melrose, D.B., 1995, Aus.J.Phys., 48, 571
- Verbunt, F. et al., 1996, A&A, 311, L9
- Seward, F.D. & Wang, Z.-R., 1988, ApJ, 332, 199
- Wei, D.M., Cheng, K.S., Lu, T., 1996, ApJ, 468, 207
- Weekes, T.C., 2000, In: *GeV-TeV Gamma Ray Astrophysics Workshop: Towards a major atmospheric Cherenkov detector VI* ed. B.L. Dingus, M.H. Salamon, D.B. Kieda: AIP Conference Proceedings, Vol. 515., p.3 (New York: AIP)
- Wózna, A. et al., 2002, *XXIInd Moriond Meeting 'The Gamma-Ray Universe'*, in press (astro-ph/0205224)
- Xia, X.Y. et al., 1985, A&A, 152, 93
- Young, M.D., Manchester, R.N., Johnston, S., 1999, Nature, 400, 848
- Zhang, B. & Harding, A.K., 2000a, ApJ, 532, 1150
- Zhang, B. & Harding, A.K., 2000b, ApJ, 535, L51
- Zhang, B. & Qiao, G.J., 1998, A&A, 338, 62